A COMPARISON OF SMALL AND LARGER MESOSCALE LATENT HEAT AND RADIATIVE FLUXES: DECEMBER 6 CASE STUDY

I. Gultepe and D. O'C. Starr
NASA, GSFC, Code 913
Greenbelt, MD 20771

A. J. Heymsfield
NCAR P.O. Box 3000
Boulder CO 80307

1. INTRODUCTION

Because of the small amounts of water vapor, the potential for rapid changes, and the very cold temperatures in the upper troposphere, moisture measuring instruments face several problems related to calibration and response. Calculations of eddy moisture fluxes are, therefore, subject to significant uncertainity.

The purpose of this study is to examine the importance of latent heat (moisture) fluxes due to small and larger mesoscale mesoscale circulations in comparison to radiative fluxes within cirrus. Scale separation is made at about 1 km because of significant changes in the structures within cirrus. Only observations at warmer than -40 C are used in this study.

The EG&G hygrometer that is used for measuring dewpoint temperature (T_d), is believed to be fairly accurate down to -40 C (Schanot, 1987). On the other hand, Lyman-Alpha (L-α) hygrometer measurements of moisture may include large drift errors. In order to compensate for these drift errors, the L-α hygrometer is often calibrated against the EG&G hygrometer (Jensen and Raga, 1991; Friehe et al., 1986). However, large errors ensue for T_d measurements at temperatures less than -40 C. The cryogenic hygrometer (Busen and Buck, 1993) frost point measurements may be used to calibrate L-α measurements at temperatures less than -40 C. In this study, however, measurements obtained by EG&G hygrometer and L-α measurements are used for the flux calculations.

2. AIRCRAFT MEASUREMENTS

Data for this case study were taken from the FIRE Cirrus II field project which took place over the Kansas region during November and December of 1991. Temperature, dewpoint, radiation and INS wind measurements from NCAR King Air for December 6 case were used in the calculations. Mixing ratio values are obtained from both EG&G and Lyman Alpha fast response hygrometers. Data sampling rate was 20Hz for the measurements used in flux calculations. The cirrus cloud formed on this day was related to an upper jet stream and short wave trough at about 300 mb. Time series of temperature and wind measurements at seven constant altitudes ranging from 6 to 9 km show that the layers close to cloud top had large w fluctuations (± 1 m s^{-1}). Broad band radiative fluxes were obtained from Eppley radiometers in both the shortwave and infrared range.

3. METHOD

This section describes the latent heat (moisture) and radiative flux calculations, and scale partition for the latent heat flux calculations.

a. Latent heat flux calculation

Mixing ratio values are calculated from both EG&G T_d and L-α hygrometer measurements. Mixing ratio q_{vE} from EG&G T_d measurements is obtained as

$$q_{vE} = \frac{\epsilon e(T_d)}{P - e(T_d)}, \tag{1}$$

where e is the saturated vapor pressure at the given dewpoint temperature, and P is the pressure.

Mixing ratio values from L-α measurements are obtained from the equations given by Buck (1976):

$$I = I_o exp(-s \sum \frac{k_i \rho_{vi}}{\rho_{vi}}), \tag{2}$$

$$V = ln(I), \tag{3}$$

where I is detector current, I_o is detector current with path length set zero, s the path length, k absorption coefficient, ρ_{vi} density of ith gas in path, and V is voltage. Vapor density then is calculated from the observed voltage (Schanot, 1987).

In our calculations, leg-averaged vapor mixing ratio values, calculated from EG&G bottom hygrometer measurements, are plotted versus constant altitude leg averaged L-α voltage (V) measurements (see Fig. 1). In this figure, the cross indicates mean values. The thin and thick lines are sounding values of the same parameters based on the L-α hygrometer q_v and EG&G q_v values, respectively. A regression line obtained from Fig. 1 is shown in Fig. 2 and it is given as

$$q_{vE} = 7.072 + 0.8036 V_{L-\alpha}. \tag{4}$$

Using perturbation theory, mixing ratio fluctuations from Eq. (4) are obtained as

$$q'_{vE} = 0.8036 V'_{L-\alpha}. \tag{5}$$

Using Eq. (5) and vertical velocity fluctuations w', time series of eddy latent heat fluxes are obtained from the following equation:

$$F = L_v w' q'_{vE} = L_v S w' V'_{L\alpha}, \tag{6}$$

where L_v is the latent heat of vaporization. S is the slope of regression line and it is equal to 0.8036 for December 6 case. Eq. (6) is used in this study to obtain time series and leg-averaged latent heat fluxes.

Scale separation within cirrus is made using a running-average technique. The calculated latent heat fluxes are thereby partitioned into those attributable to scales less than and greater than 1 km.

b. Radiative flux profiles

Average radiative fluxes of both IR and SW irradiances over constant altitude flight legs are obtained from the Eppley up and down looking radiometers. Radiative flux divergence for each layer is calculated from radiometer measurements.

4. RESULTS AND CONCLUSIONS

a. Comparisons of latent heat and radiative fluxes

Small and larger scale latent heat flux time series calculated over leg 1 and net radiative flux data are shown in Fig. 3 and Table 1, respectively. Mean values of latent heat fluxes (see Table 2) are found to be very small compared to radiative flux values. Although mean values are small, turbulent fluxes at individual points (see Fig. 3) are found to be comparable with net radiative fluxes (see Table 1) in any layer within cirrus. This shows that inhomogeneity within cirrus can be very important for trasferring heat and moisture in the horizontal and vertical. Heating rates corresponding to IR, SW, and IR+SW radiation are given in Fig. 4. Standard error of

IR and SW radiative fluxes are approximately ±5 and ±10 W m^{-2} (Gultepe and Starr, 1993), respectively.

Time series of latent heat fluxes (Fig. 3) show that small scale processes (scales less than 1 km) can have a significant contribution to mean latent heat fluxes (see Table 2). Table 2 shows the latent heat fluxes estimated for upward and downward directions in two different scales. The ratio R between small scale and large scale contributions is equal to $(w'q')_S/\ (w'q')_L$. Results show that small scale flux contribution is approximately 30%. Under the turbulent conditions which are indicated in legs 2 and 6, small scale contribution is about 70%.

b. Effects of moisture fluxes on ice crystal concentration

The typical values of mixing ratio and vertical velocity fluctuations are approximately 0.02 g m^{-3} and 0.20 m s^{-1}, respectively. Moisture flux rate then is obtained from Eq. (6) and it is about 0.004 g m^{-2} s^{-1}. Using Δt time period equal to 10 s, the transferred mass rate, ΔM_t, is estimated to be 0.04 g. If we assume that a layer just above the constant leg is saturated with respect to ice, using a mono-type particle size distribution with spherical crystal shape, and assuming that transferred moisture totally changes into ice, the number of ice crystals being formed is estimated as follows:

$$N_i[\frac{particles}{cm^2}] = \frac{\Delta t \times \Delta M_t \times 10^{-4}}{(4/3)\pi r_e^3 \rho_i} \tag{7}$$

where ρ_i is the ice crystal density. Using equivalent particle size r_e=10 μm and ρ_i=0.8 g cm^{-3}, N_i is estimated to be approximately 1.2×10^6 particles cm^{-2} for a 10 second time period. Even though this number may include large error (about %20-30), the results showed that small scale eddy moisture fluxes can play an important role in cirrus development.

ACKNOWLEDGEMENT

This work was supported by the NASA Office of Space Science and Applications under the direction of Dr. John T. Suttles. The first author during this work held a National Research Council Research Associateship at Climate and Radiation Branch of the NASA Goddard Space Flight Center in Greenbelt Maryland.

REFERENCES

Buck, A. L., 1976: The variable-path Lyman-alpha hygrometer and its operating characteristics. *Bull. Amer. Meteor. Soc.*, 57, 1113-1118.

Busen R., and A. L. Buck, 1993: The CR-1 cryogenic hygrometer on board the DLR falcon: installation, performance tests, and examples of measured data. *8th symposium on Meteor. Obser. and Instrumen.*,73rd AMS Annual Meeting, january 17-22.

Friehe, C. A., Grossman R. L. and Y. Pann, 1986: Calibration of an airborne Lyman-Alpha Hygrometer and measurement of water vapor flux using a thermoelectric hygrometer. *J. Atmos. Ocean. Tech.*, 3, 299-304.

Gultepe, I, and D. O'C. Starr, 1993: Dynamical structure and turbulence in cirrus clouds: Aircraftobservations during FIRE I. *J. Atmos. Sci.*, submitted.

Jensen, B. J., and G. B. Raga, 1993: Calibration of a lyman-α sensor to measure in-cloud temperature and clear-air dewpoint temperature. *J. Atmos. Ocean. Tech.*, 10, 1-26.

Schanot, A., 1987: An evaluation of the uses and limitations of a Lyman-Alpha hygrometer as an operational airborne humidity sensors. *6th symposium on Meteor. Obser. and Instrumen.*, january 12-16, New Orleans, La., 257-260.

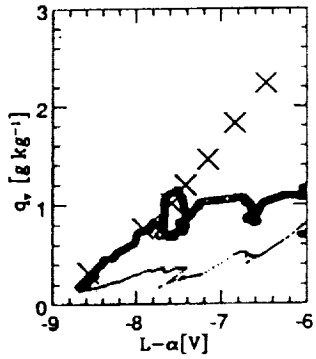

Fig. 1: Shows vapor mixing ratio versus L-α voltage. The crosses are for mean values over constant altitude flight legs. Other lines are for aircraft sounding values.

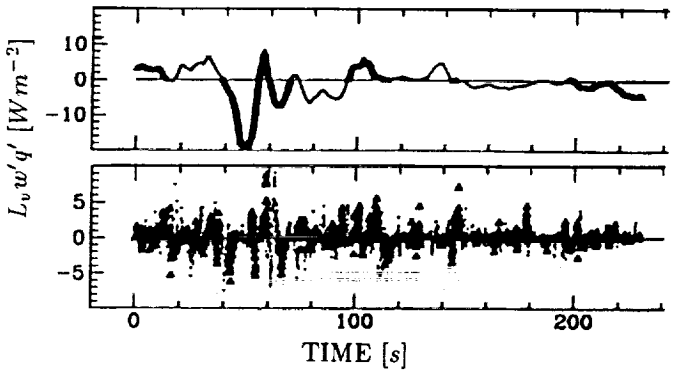

Fig. 3: Top and bottom panels shows time series of small and larger scale eddy latent heat fluxes along leg 1 (at 6.0 km) for December 6 case, respectively.

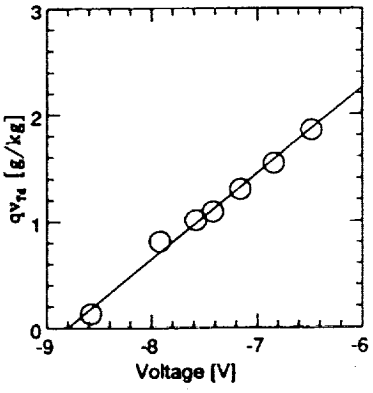

Fig. 2: Shows vapor mixing ratio versus voltage. The circles are for mean values at constant altitudes. The straight line is best fit for the mean values.

Z (km)	IR^u	IR^d	SW^u	SW^d	layer	IRnet	SWnet
6.0	286.3	240	10.9	153.4	1	-2.5	43.1
6.3	279.9	231.1	29.73	215.3	2	-32.1	16.4
6.6	275.0	194.1	63.02	278.6	3	3.5	4.1
6.9	264.6	188.2	73.93	280.0	4	-31.6	14.6
7.2	260.3	152.3	84.6	305.3	5	-23.3	95.7
7.5	256.3	125.0	118.1	434.5	6	-10.9	33.0
8.8	230.6	88.2	193.8	543.5			

Table 1: Averaged IR and SW irradiances (W m^{-2}) versus constant altitudes. Last two columns are gain or loss for each layer.

Table 2: Small and large scale eddy latent heat fluxes (F_S and F_L) for upward (+) and downward (-) directions. The R shows ratio between small and large scale fluxes. The F_{max} is the maximum individual flux value (W m^{-2}) on a leg.

Z (km)	F_L^+	sd	F_L^-	sd	F_S^+	sd	F_S^-	sd	R^+	R^-	F_{max}
6.0	2.4	1.9	3.2	3.9	0.8	1.1	0.8	1.0	0.34	0.24	20
6.3	1.4	1.4	0.9	1.0	0.9	1.5	0.6	1.0	0.64	0.73	8
6.6	1.8	1.3	2.1	3.1	0.3	0.4	0.2	0.3	0.14	0.10	-15
6.9	1.8	2.1	1.3	1.5	0.2	0.3	0.2	0.3	0.13	0.16	10
7.2	1.2	0.8	1.5	1.5	0.2	0.3	0.2	0.4	0.16	0.15	-8
7.5	2.7	5.1	1.4	1.3	1.4	4.0	1.0	3.5	0.53	0.73	20
8.8	6.1	8.7	1.2	1.2	0.3	0.5	0.3	0.4	0.06	0.26	20

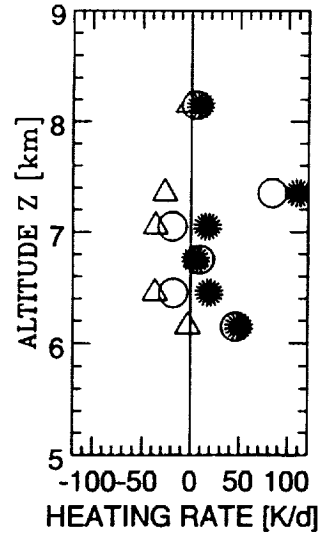

Fig. 4: Potential heating rates for IR (triangles), SW (stars), and IR+SW (circles) radiation.